Research Square

Preprints are preliminary reports that have not undergone peer review.
They should not be considered conclusive, used to inform clinical practice,
or referenced by the media as validated information.

Revised Methodology for Fluence Determination and Sample Loss Correction in Near-Field, Long-Exposure Bench-Scale UV LED Experiments

Rania A. Elsebai
Dalhousie University
Jessica L. Bennett
Dalhousie University
Sean A. MacIsaac
Dalhousie University
Rich M. Simons
Aquisense Inc
Amina K. Stoddart
Dalhousie University
Graham A. Gagnon
Graham.Gagnon@dal.ca
Dalhousie University

Article

Keywords: UV LEDs, Photolysis, Fluence, Disinfection, Advanced Oxidation, Water Treatment

Posted Date: November 20th, 2026

DOI: https://doi.org/10.21203/rs.3.rs-11623515/v1

License: This work is licensed under a Creative Commons Attribution 4.0 International License. Read Full License

Additional Declarations: Competing interest reported. In accordance with journal disclosure policies, we acknowledge that Rich Simons is employed by Aquisense Inc. which provided partial funding for this work. The remaining authors declare no competing interests.

Abstract

Ultraviolet light-emitting diodes (UV LEDs) are increasingly used in bench-scale water treatment research, but conventional fluence determination protocols developed for mercury lamps may not adequately represent near-field and long-exposure experiments typical of UV LEDs. This work evaluated the limitations of conventional approaches and developed a practical framework for fluence determination and sample loss correction in bench-scale UV LED experiments. The framework was evaluated using UV LED photodegradation experiments on compounds with differing photostability and action spectra (estrone (E1), 17α-ethinylestradiol (EE2), and caffeine). Among the factors assessed, beam divergence correction (i.e., divergence factor) had the greatest impact on fluence determination, with the revised approach changing average fluence rate by 15.9% under the closest near-field condition. Sample loss correction changed fluence-based degradation rate constants by 2.1%, 4.6%, and 93.9% for E1, EE2, and caffeine, respectively, with effects increasing with exposure duration and volume drop, particularly for more photostable compounds. Based on these findings, a decision framework was developed to identify when conventional methods remain appropriate and when revised calculations are required. This research provides a practical basis for more reliable fluence and degradation kinetics measurements in near-field and long-duration bench-scale UV LED studies or for other light sources operating under cited conditions.

1.0 Introduction

Ultraviolet (UV) light-based technologies are widely applied in water treatment research for microbial inactivation and degradation of organic contaminants[1–3]. UV LEDs have emerged as a promising alternative to traditional mercury-based UV systems, primarily because they are compact, capable of instantaneous operation, inherently mercury-free, and offer targeted treatment through wavelength tunability[4,5]. The effectiveness of UV LEDs has been demonstrated across a range of use cases, including disinfection[2,5], chemical degradation[3,6], and, more recently, municipal-scale water treatment[4,7]. The growing body of research indicates that UV LEDs have progressed beyond bench-scale and point-of-use (POU) applications and towards alternative use cases including municipal-scale and high-fluence treatment scenarios.

A central parameter connecting bench-scale UV experiments with practical reactor performance is UV fluence, commonly referred to as UV dose, which is a measure of the amount of light passing through a given volume of space, per unit area, over time[8,9]. Expressing microbial inactivation or contaminant degradation as a function of fluence, rather than exposure time, allows treatment kinetics to be compared across different light sources, irradiances, and reactor configurations[3,10,11]. Accurately determined bench-scale fluence-response relationships support reliable UV auditing studies, which assess the performance, delivered fluence, and operational limitations of full-scale UV reactors[12]. This ultimately supports the evaluation and scale-up of UV treatment systems. For example, MacIsaac et al. (2024) demonstrated the operation of a municipal-scale 280 nm UV LED reactor for wastewater disinfection and reported that its delivered fluence was consistent with performance predicted through a preceding bench-scale UV-auditing study[4]. Consequently, errors in bench-scale fluence determination can affect not only calculated kinetic parameters but also the interpretation and practical scale-up of laboratory findings.

The standard method for fluence determination in bench-scale UV experiments was first presented by Bolton & Linden (2003)[8]. This protocol was principally developed for low-pressure (LP) UV lamps, which emit nearly monochromatically at 253.7 nm, and medium-pressure (MP) UV lamps, which emit polychromatically across a wide region of the electromagnetic spectrum[3,8]. Furthermore, this protocol was developed using simplifying assumptions appropriate to the conventional collimated-beam configurations considered. While this protocol has frequently been applied to UV LED systems[3,13,14], modifications are often necessary to adjust to fundamental differences in light delivery between mercury-based lamps and LEDs[10,15]. UV LEDs are narrow-band polychromatic light sources, with distinct radiation profiles (e.g., balloon- or heart-shaped)[10,15] and full width half maximum (FWHM) of approximately 10–20 nm[10,15,16]. Furthermore, UV LEDs may exhibit lower radiant power (particularly for lamps that emit light within the UV C spectrum[1,10]). As a result, samples are sometimes placed close (1–10 cm) to the UV LED device during UV exposure, resulting in non-collimated beam behavior and potentially reducing the accuracy of conventional fluence correction factor equations[10,15,17]. Long exposure times may also be required to reach high target fluences (> 1000 mJ cm^{-2}) which are sometimes required to degrade photostable chemical contaminants[3,6]. Exposure periods may extend for several hours when these fluences are achieved using an open, low-power UV LED system, thus increasing the potential for sample loss through evaporation. Assuming constant experimental conditions throughout the exposure period may introduce errors into both delivered fluence calculations and measured degradation kinetics since these changes in sample volume occur during the fluence delivery window of time.

Several studies have introduced methods for UV fluence determination specific to UV LEDs that account for polychromatic emission, non-collimated beam behavior, and angular radiation profiles[10,15,17]. However, these methods have primarily been evaluated for single-chip systems or relatively short microbial-inactivation experiments. The combined effects of multi-chip irradiance distributions, near-field operation, and changing sample conditions during long exposure periods have received less attention. In particular, the effects of sample loss on both fluence determination and measured contaminant concentrations are commonly overlooked. A practical methodology is therefore needed to evaluate the optical characteristics of near-field, multi-chip UV LED systems and account for time-dependent changes in sample conditions during long-duration experiments.

Accordingly, this study developed and evaluated a revised framework for fluence determination and sample-loss correction in near-field, multi-chip, bench-scale UV LED systems requiring long exposure times to achieve target fluences for effective chemical degradation. Rather than developing a complete optical model of UV LED emission, the focus is on improving practical calculations of delivered fluence and degradation kinetics under conditions where sample volume and liquid depth change over time. The proposed framework was evaluated using UV LED photodegradation experiments with three environmentally relevant trace organic contaminants (TrOCs) in water with different photostability: E1, EE2, and caffeine.

2.0 Materials and Methods

2.1 Bench-Scale Apparatus

A typical bench-scale collimated beam set-up consists of a UV beam in a housing with an aperture that forms a quasi-collimated UV beam directed vertically with respect to the surface of the sample being irradiated[8,9]. A shutter and timer are integrated with the setup to control exposure time[8,9]. Figure 1 shows a photo of the bench-scale UV LED beam experimental set-up used for this study, optimized for repeatability and reproducibility. The setup consists of: (1) a grooved base that locks the positioning of setup components across experiments, (2) a stir plate that ensures the sample is well-mixed throughout the experiment, (3) lab jacks for height adjustments (i.e., moving the UV LED beam away from or closer to sample surface), (4) a sample Petri dish with a Teflon® coated stir bar inside, (5) levelled plate to position beam above sample service, (6) the UV LED beam, and (7) the UV LED control panel. The UV LED beam depicted in Fig. 1 is the AquiSense PearlBeam unit that is equipped with three independent 235 nm channels. This instrument was used for all experiments in this study. Adequate sample stirring was maintained during UV exposure to ensure uniform fluence delivery across the sample volume. Stirring was performed at low speeds (100–300 rpm) using a small stir bar (10–12 mm diameter for 50–60 mm diameter Petri dish) to prevent vortex formation, which can cause light scattering[8].

2.2 Determination of Incident Irradiance, Correction Factors, and Average Fluence Rate

The centre point irradiance (E_0), reported in units of W m^{-2} or mW cm^{-2}, is the amount of light incident at the centre on a sample surface per unit area[8]. For this study, irradiance was measured using an Ocean Optics SR4 series miniature spectrometer (SR-4UVV240-50) equipped with a CC-3-DA cosine corrector. During measurements, the detector head was positioned at the center under the UV LED beam, at the same displacement between the sample surface and UV LED beam implemented for this study (29.75 mm). The average fluence rate (E'_{avg}), calculated using Eq. 1 and reported in units of W m^{-2} or mW cm^{-2}, is the average amount of light passing through a sample volume per unit area[8].

$$E'_{avg} = E_0 \times PF \times WF \times DF \times RF$$

1

Here, PF is the Petri factor, which corrects for the variability in irradiance across the sample surface plane with respect to the center irradiance (E_0)[8]. WF is the water factor, which corrects for the reduction in irradiance arising from absorbance by the sample medium as UV light passes through it[8]. DF is the divergence factor, which corrects for the reduction in irradiance of the UV light as it diverges from the sample surface to the sample bottom[8]. RF is the reflection factor, which corrects for the loss in irradiance resulting from light reflecting off sample surface[8]. The methods used to determine these correction factors are described in the subsequent sections below (sections 2.2.1–2.2.4). The sensor factor was not accounted for here as a spectrometer was used for irradiance determination. A spectrometer should be used for characterizing UV LED systems as it can cover the entire emission spectrum of the LED system, resulting in higher measurement accuracy compared to radiometers[18].

2.2.1 Petri Factor

The purpose of the PF is to determine the average irradiance across the sample surface (E_{avg}) from a single irradiance measurement at the center of the sample plane[8]. This means that for each experimental set-up, irradiance measurements must be taken across the entire sample area only once, which enables calculation of the PF by dividing the irradiance measured at each point on the sample plane by E_0 (Eq. 2)[8]. Then, for all future experiments under the same experimental conditions (i.e., same UV source and displacement between sample surface and UV source), the irradiance only needs to be measured at the center, after which the average irradiance across the entire sample surface can be determined by multiplying E_0 by PF (Eq. 2).

$$PF = \frac{E_{avg}}{E_0}$$

2

For this study, the PF was determined by measuring the irradiance across a two-dimensional Cartesian grid at 5 mm increments in the x-y direction over the entire surface area of the sample plane at the same displacement between the UV beam and sample surface during measurements (29.75 mm). Care should be taken to take the irradiance measurements across a plane parallel to the top of the fluid to be irradiated, and not the base or top of the container holding the sample. Each measurement point was assigned a square grid cell with a side length equal to the measurement spacing (5 mm). To account for the circular geometry of the Petri dish (54 mm internal diameter), the area of each grid cell falling within the sample surface was calculated. Cells entirely within the Petri dish were assigned their full area (25 mm^2), while cells overlapping with the edge of the Petri dish were assigned the corresponding partial area depending on percentage overlap. Cells located entirely outside the sample surface area were excluded. SI Text 1 provides the area and irradiance measurements for each grid across sample surface. The average irradiance across the entire sample surface (E_{avg}) was then calculated as an area weighted average as represented by Eq. 3, where E_i is the irradiance measured at grid point i (μW cm^{-2}), A_i is the corresponding grid cell area within the sample surface (mm^2), and n is the total number of grid cells. The PF was then determined using Eq. 2. A spreadsheet is provided in the supplementary information (SI) that automatically calculates the PF using this approach based on user input data for Petri dish diameter, irradiance measurements across sample surface, and spacing between irradiance measurements.

$$E_{avg} = \frac{\sum_{i=1}^{n} E_i A_i}{\sum_{i=1}^{n} A_i}$$

3

Using this approach, the PF was measured to be 0.727 for this study. Ideally, the PF should not be lower than 0.9 in a well-designed collimated beam setup[8,9]. However, due to the non-collimated nature of some bench scale UV LED systems, maintaining a PF ≥ 0.9 may not always be possible, and several bench scale UV LED studies reported PF values below 0.9[19–22]. Hence, it was assumed that so long as the sample is well-mixed during irradiation, an even exposure will be achieved across the sample volume regardless of PF value. This was also noted by Keshavarzfathy et al. (2020), who ensured gentle mixing of samples for at least 3 minutes during irradiation to account for the non-uniform fluence rate distribution across sample volume[17].

2.2.2 Water Factor

The WF was determined using two approaches for this study, one assuming monochromatic (mono) emission (single wavelength emission) and the other accounting for the polychromatic (poly) emission (emission across range of wavelengths). This was done to assess the impact of assuming monochromatic emission at peak wavelength for UV LED beams, which is frequently implemented in literature [23–26]. The monochromatic WF was determined using the same using the procedure proposed by Bolton & Linden (2003)[8], as outlined in the SI Text 2. For polychromatic UV beams, Bolton & Linden (2003) recommend the WF correction be made over a narrow band (1–5 nm) range of wavelengths[8]. The procedure outlined below was used for determination of the polychromatic WF ($WF\left(\lambda\right)_{poly}$)[8,10]. An Excel spreadsheet is also included in the SI to automatically calculate $WF\left(\lambda\right)_{poly}$ following the steps below.

1. The UV LED beam emission spectrum (intensity vs. wavelength) was measured using an Ocean Optics SR4 series miniature spectrometer (SR-4UVV240-50) equipped with a CC-3-DA cosine corrector. The wavelength integration range (220–250 nm) was selected based on the measured emission spectrum to encompass the LED emission band, with the integration limits corresponding to regions where the spectral intensity approached a flat baseline, as demonstrated by Figure SI-1 in SI Text 3. For other UV LED sources, the integration range should be adjusted accordingly based on their respective emission spectra.
2. The absorbance of the sample being irradiated was measured using the Shimadzu LabSolutions UV-Vis spectrophotometer (model UV-2600i) over the spectral emission range of the UV LED beam (220–250 nm) at 1 nm increments.
3. The UV LED emission spectrum was normalized by dividing the irradiance at each wavelength against the summation of the irradiance throughout all wavelengths in the emission spectrum (Eq. 4):

$$E_{norm}\left(\lambda\right)=\frac{E\left(\lambda\right)}{\sum_{\lambda}E\left(\lambda\right)}$$

4

1. $WF\left(\lambda\right)_{poly}$ was calculated by taking the summation of the product of $E_{norm}\left(\lambda\right)$ and WF at each wavelength (Eq. 5). The summation was made over 1 nm wavelength increments until all wavelengths in the emission spectrum (220–250 nm) were accounted for.

$$WF_{poly}=\sum_{\lambda}WF\left(\lambda\right)E_{norm}\left(\lambda\right)$$

5

Ideally, the effects of WF and DF should be considered together[8]. Bolton & Linden (2003) suggested that the errors associated with treating these factors independently are negligible for path lengths below 5 cm[8]. Although the sample depth in the present study falls within this range (2.2 cm), the applicability of this assumption to near-field configurations has not been established and the WF and DF were treated independently in this study. Any potential errors associated with not combining these factors were not quantified but could be an additional source of variability. Furthermore, when operating under near-field conditions, as implemented for this study, incident angle effects may not be negligible for WF determination. This is because, when UV rays are hitting the sample at different incident angles rather than normal to the surface, the sample path length will be longer, which results in more absorbance and lower transmitted energy, hence impacting the WF[15]. At the maximum incident angle associated with the experimental set-up implemented for this study (42.23°), refraction at the air-water interface reduced the angle of light propagation in water to 29.33°, resulting in only a 0.04% difference in WF relative to normal incidence (SI Text 4). Figure 2 illustrates the effect of incident angle (0–45°) on WF for UV transmittance (UVT) values ranging from 80% to 95% and a sample depth of 1 cm. The relative difference in WF remained below 5% across all evaluated conditions, increasing with higher incident angles and lower UVT. However, since the impact of incident angle on WF depends on sample depth and UVT, these effects should be evaluated for each experimental configuration.

2.2.3 Divergence Factor

The DF was determined using three approaches for this study. The first approach measures the DF experimentally using the definition-based formula (Eq. 6), where L is the distance between the UV source and sample surface, l is the sample depth in Petri dish, $E_{avg}\left(L\right)$ is the average irradiance across the sample surface at displacement L from UV source and sample surface, and $E_{avg}\left(x\right)$ is the average irradiance across the sample surface at displacement x from UV source and sample surface[10]. The integral in Eq. 6 ($\int_{L}^{L+l}E_{avg}\left(x\right)\,\mathrm{hspace}\{0.17\mathrm{em}\}dx$) was solved using trapezoid integration.

$$DF=\frac{\frac{1}{l}\int_{L}^{L+l}E_{avg}\left(x\right)\,\mathrm{hspace}\{0.17\mathrm{em}\}dx}{E_{avg}\left(L\right)}=\frac{\int_{L}^{L+l}E_{avg}\left(x\right)\,\mathrm{hspace}\{0.17\mathrm{em}\}dx}{l\,\mathrm{hspace}\{0.17\mathrm{em}\}E_{avg}\left(L\right)}$$

6

The second approach uses the standard formula proposed by Bolton & Linden (2003)[8] (Equation SI-8 in SI Text 5). This formula assumes negligible incident angle of radiation effects (i.e., quasi-collimated), and was derived from the inverse-square law (ISL), which is used for determining irradiance hitting the sample surface at source-to-sample displacements more than 4 to 5 times the aperture diameter of the UV beam (i.e., far-field distance)[8,15,27]. At such distances, the error in using the ISL to predict irradiance is within 1%[15,27]. However, this 4 to 5 times rule of thumb is specific to line or circular shape UV sources with Lambertian emission (i.e., uniform emission in each direction)[15,27].

The 235 nm UV LED unit used for this study has a heart-shaped emission profile. Hence, the 4 to 5 times rule of thumb may not be applicable for accurately determining the far-field distance required to achieve within 1% error when using the ISL for irradiance prediction[15,27]. Several studies noted that for UV LED systems, the far-field distance required to maintain within 1% error when using the ISL is at least 7 times the maximum diagonal distance between the UV LED chip array in the beam (equivalent to approximately 20 cm between the UV source and sample surface)[10,28]. For the 235 nm UV LED system used for this study, the maximum diagonal distance between the LED chip array in the beam is 2.5 cm, which means a distance of at least 17.5 cm between the LED and sample surface is required to achieve quasi-collimated conditions and use the standard DF formula (Equation SI-8 in SI Text 5). Here, the distance from the UV LED to sample surface is determined from the semiconductor crystal that forms the emitting element of the LED, not the external package.

However, as this UV LED beam has low radiant power (average centre-point intensity of 65.5 μW cm^{-2} at 29.75 mm displacement from beam), it must be placed at close distances to sample surface without collimation (i.e., near-field). For this study, the displacement between the UV LED chips and sample surface was 29.75 mm. Under these near-field conditions, the ISL is invalid, and the incident angle of radiation must be considered to account for non-collimated beam behaviour. Therefore, an alternative equation for DF determination was developed by AquiSense Inc. that accounts for the non-collimated behavior of the UV LED beam under near-field conditions (Eq. 7). Here, D is the diameter of the sample Petri dish, L is the vertical displacement between the UV source and sample surface (measured from the semiconductor crystal that forms the emitting element of the LED, not the external package), and l is the depth of sample inside the Petri dish. A spreadsheet is provided in the SI to automatically calculate DF using Eq. 7 based on user input values for D, L, and l. The derivation of Eq. 7, presented in SI Text 6, assumes a circular irradiance plane and follows from the average of the solid angles (Ω) subtended by the sample surface plane ($\Omega_{SP,surface}$) and the parallel plane at the bottom of the sample ($\Omega_{SP,bottom}$), when viewed from the mid-point of the UV source. The refraction of the transmitted rays between the air-water interface was not accounted for in the derivation of this formula. The conventional and revised DF formulas (Equation SI-8 and Eq. 7, respectively) were evaluated and compared against the experimentally measured DF results (Eq. 6).

$$DF = \frac{1 - \frac{\sqrt{(L+l)^2+\left(\frac{D}{2}\right)^2} - \sqrt{L^2+\left(\frac{D}{2}\right)^2}}{l}}{1 - \frac{1}{\sqrt{\left(\frac{D}{2L}\right)^2+1}}}$$

7

2.2.4 Reflection Factor

The Bolton & Linden (2003)[8] protocol assumes a constant 0.975 value for RF, which was determined by assuming beam incidence normal to sample surface and air and water as the two media[8]. Furthermore, the average refractive indices in the 200–300 nm region for air (1.000) and water (1.372) were used to calculate this 0.975 RF value[8]. However, considering the refractive index of air and water vary with wavelength, then RF will also vary with wavelength and not remain constant at 0.975. Furthermore, assuming beam incidence normal to sample surface is only applicable to collimated systems. Under near-field experimental conditions, as the one assessed for this study, the UV light will hit the sample surface at different incident angles, which will impact the RF.

Therefore, a sensitivity assessment was performed to evaluate the impact of wavelength and incident angle variability on RF. Figure 3 and Table SI-1 in SI Text 7 present RF data at the air-water interface at varying incident angles (0–45°) and wavelength ranges (200–400 nm). The deviation of RF from the conventional 0.975 value was observed to increase at lower wavelengths and higher incident angles, with a maximum change of 1.52% in the RF observed under these conditions relative to the conventional 0.975 value. At the maximum incident angle associated with the experimental set-up implemented for this study (42.23°), a negligible 0.57% change in the RF was observed relative to the standard 0.975 value (SI Text 4.2). Accordingly, the conventional RF value of 0.975 was considered applicable for this study. For other experimental configurations, the applicability of this approximation should be evaluated by considering the effects of wavelength and incident angle, with relative differences of ≤ 1% from the conventional RF value considered negligible[10,15].

2.3 Determination of Fluence ($\varvec{F}$) Using the Trapezoid Integration Method During Long-Run Experiments

Fluence (F) is calculated as E_{avg} integrated over exposure time (t), in seconds[8]. If E_{avg} is constant throughout experiment time, then fluence can be calculated by multiplying E_{avg} by exposure time[8]. However, E_{avg} is not necessarily constant across the window of UV exposure due to evaporative sample losses. Considering these factors is especially critical during long exposure experiments where the change in sample volume or E_{avg} during experiments exceeds 5%[3,29]. Therefore, a more accurate approach for fluence determination is presented below.

The proposed method involves determining E_{avg} at different exposure times during the experiment and then implementing trapezoid integration to calculate the delivered fluence. To determine E_{avg} at different exposure times, it is necessary to track changes in sample volume over time and then use this data to

calculate the displacement between sample surface and UV beam, and sample depth, at different exposure times. In the E_{avg} formula (Eq. 1), changes in displacement impact E_0 and DF, and changes in sample depth impact DF and WF. Hence, by calculating the displacement and sample depth at different timepoints, the corresponding E_0, WF, and DF can be determined at each timepoint. From there, E_{avg} at different timepoints can be calculated using Eq. 1.

Section 2.3.1 outlines the procedure for tracking changes in sample volume over time, which enables calculating displacement and sample depths at different exposure times. Section 2.3.2 introduces an irradiance-displacement decay model for the UV LED beam used in this study, which allows for calculating E_0 at different displacements during the experiment. Section 2.3.3 highlights the trapezoid integration approach for fluence determination.

2.3.1 Correcting for Sample Loss Throughout Bench-Scale Experiments

Sample evaporation and intermittent sampling for analysis contribute to sample loss throughout bench-scale UV LED experiments. Monitoring sample loss throughout experiments is critical as it impacts the WF (sample depth l decreases) and the DF (l decreases and displacement L increases) and, as previously mentioned, changes E_0. The procedure implemented for tracking sample loss during experiments is presented in the SI Text 8. By calculating changes in displacements and sample depths at different exposure times during the experiment using the obtained sample mass data, the corresponding E_0, WF (Equation SI-1), and DF (Eq. 7) can be determined at the associated exposure times. The procedure for determining E_0 at different sample surface displacements from the beam is outlined in section 2.3.2.

2.3.2 Prediction of Irradiance Change with Displacement from UV LED Beam

An irradiance-displacement decay model was derived for the 235 nm UV LED system used for this study, as outlined below, which can be used to understand and quantify the effect of sample loss on E_0. This procedure can be applied to other bench-scale UV LEDs, as well as conventional UV (e.g., mercury-based) and alternative source (e.g., krypton-chloride) systems operating under near-field conditions in which the ISL does not apply.

Step 1: Measure E_0 at different displacements from the beam using a spectroradiometer or radiometer. Table SI-2 in SI Text 9 presents E_0 spectroradiometer measurements at different displacements from the 235 nm UV LED beam used for this study. It is recommended that ≥ 5 displacement points within the range of interest are measured.

Step 2: Determine the best mathematical model to describe the UV LED irradiance-displacement decay using the non-linear least squares (NLS) regression function in R. The R code used for this study is published in GitHub for reference[30].

Two decay models, inverse-square and exponential, were evaluated for this study, as presented in SI Text 9. Based on validation studies of both models using the 235 nm UV LED beam (SI Text 9), the inverse-square model was selected for modelling the UV LED beam irradiance decay with displacement. The final fitted equation from the inverse-square model is outlined by Eq. 8 below, where $E(L)$ is the centre point irradiance (μW/cm²) predicted from the model at a displacement L (mm) from the beam.

$$E(L) = \frac{133900}{(L + 12.17)^2} - 5.582$$

8

Due to the beam decay over time, variability in E_0 was observed at different displacements relative to the derived inverse-square irradiance-displacement decay model (Eq. 8). As a result, a procedure was developed in which a scaling factor, k, is applied to the main Eq. 8 model to correct for differences in E_0 measured at the start of each experiment (Step 3).

Step 3: Determine scaling factor (k).

A scaling factor should be determined and applied to Eq. 8 to predict irradiance at different displacements throughout the experiment, as demonstrated below.

- Measure E_0 at the start of every experiment at L_0 using a spectroradiometer or radiometer.
- Substitute L_0 to Eq. 8 to determine the model-predicted E_0 at L_0.
- Compute k by dividing the measured irradiance by that predicted by Eq. 8 at L_0, as follows: $k = \frac{E(L_0)_{measured}}{E(L_0)_{Equation\ 8}}$
- Apply k to Eq. 8 to get the actual predicted irradiance at different displacements L throughout the experiment (Eq. 9).

$$E(L)_{pred} = k\left[\frac{133900}{(L + 12.17)^2} - 5.582\right]$$

9

Validation of this procedure is described in SI Text 9.

2.3.3 Trapezoid Integration Method for UV Fluence Determination

Using the sample loss tracking approach outlined in section 2.3.1, it is possible to calculate WF at different sample depths over time using Equation SI-1 and calculate DF at different sample surface to beam displacements and sample depths using Eq. 7. Furthermore, changes in E_0 over time can be calculated

from the associated changes in displacement using Eq. 9, as outlined in section 2.3.2. As previously noted, by calculating E_0, WF, and DF at different exposure times, $\mathrm{E}_{\mathrm{avg}}^{\prime}$ at different timepoints can be determined using Eq. 1. From there, a more accurate delivered fluence can be calculated accounting for sample loss by integrating changes in $\mathrm{E}_{\mathrm{avg}}^{\prime}$ over exposure time using the trapezoidal integration approach, as outlined by Figure SI-6 in SI Text 10. In this approach, the exposure time is divided into discrete time intervals corresponding to target fluence checkpoints.

The fluence accumulated over each time interval, ΔF_i, can be computed using the trapezoid integration method (Eq. 10), where E_i and E_{i+1} are the average fluence rates at the beginning and end of the interval i, and Δt_i is the elapsed time between the two checkpoints.

$$\Delta F_i = \frac{E_i + E_{i+1}}{2} \Delta t_i$$

10

The total fluence delivered to the sample, F_{total}, can then be calculated by summing the fluence delivered across all time intervals i (Eq. 11).

$$F_{total} = \sum_i \Delta F_i$$

11

An Excel spreadsheet is provided in the SI that automatically calculates the delivered fluence using the trapezoid integration method following the instructions outlined in this section.

2.4 Procedure for Correcting Experimental Concentration

The sample solution evaporates over the exposure time during typical bench-scale UV experiments, resulting in measured experimental sample concentrations to be overestimated. An example of this is depicted by Figure SI-7 in SI Text 11, which shows the concentration of a 10 µg L^{-1} caffeine sample in 2 mM phosphate buffer (pH 7) increasing over time (dark experiment).

Therefore, a formula (Eq. 12) was derived to correct for the artificial increase in measured experimental concentrations resulting from sample evaporation. The corrected sample concentration at time t ($C_{SAM,\ corrected}(t)$) can be calculated by multiplying the experimentally measured sample concentration at time t ($C_{SAM,\ meas}(t)$) by the ratio of the sample volume at time t after accounting for sample evaporation alone (i.e., excluding volume removed by aliquoting) to the sample volume at time $t = 0$ (i.e., $V_{SAM}(t) / V_{SAM}(0)$). Only volume loss attributed to sample evaporation was accounted for in Eq. 12 as volume loss from aliquot removal does not impact the sample concentration for a well-mixed sample (aliquot removal decreases both sample volume and analyte concentration in sample proportionally). By contrast, for low-volatility or non-volatile compounds, primarily water is lost from the system during evaporation, with negligible analyte loss due to the low volatility of the target compound, hence resulting in an artificial increase in sample concentration.

$$C_{SAM,\ corrected}(t) = C_{SAM,\ meas}(t) \times \frac{V_{SAM}(t)}{V_{SAM}(0)}$$

12

Sample volumes throughout the experiment were determined by tracking sample mass and aliquot volumes at different exposure times and converting to volume by dividing by sample density, as previously described in section 2.3.1. The derivation and validation of Eq. 12 is outlined in SI Text 11. Eq. 12 assumes negligible analyte loss from evaporation (i.e., primarily water evaporates, and analyte degradation occurs solely due to UV exposure) and is therefore only applicable for low-volatility or non-volatile compounds.

2.5 Validation Experiment Details

The proposed methods outlined above were validated through bench-scale experiments using the 235 nm UV LED beam. Three compounds were selected for validation: E1, EE2, and caffeine. These compounds were selected because they are environmentally relevant TrOCs in water with differing photostability. Their different degradation behaviors enabled the proposed methodology to be evaluated over a range of exposure durations and associated sample loss conditions. The validation experiments were divided into two phases. The first phase evaluated the impact of the updated correction factor equations for WF, which accounts for polychromatic emission, and DF, which accounts for non-collimated beam behavior under near-field conditions, on the determination of $\mathrm{E}_{\mathrm{avg}}^{\prime}$ using caffeine as the target compound. The second phase evaluated the impact of sample loss on fluence determination and degradation kinetics using the proposed trapezoidal integration approach for fluence determination and the method for evaporation correction of experimentally measured concentrations. All three compounds (i.e., E1, EE2, and caffeine) were evaluated in this phase, allowing the proposed methods to be assessed over a range of fluences and exposure times. Details on chemicals and reagents used, equipment specifications, experimental procedures, and analytical methods are outlined below. Experiments were performed in triplicate to assess experimental variability.

2.5.1 Chemicals and Reagents

Caffeine

ACS-grade caffeine powder and 1 g L^{-1} caffeine-$^{13}C_3$ internal standard in methanol was sourced from Sigma-Aldrich. 100 mg L^{-1} caffeine stock solutions (for spiking experiments) were prepared from the neat caffeine powder in water (10 mg in 100 mL). A 1 mg L^{-1} caffeine working solution (for making calibration

standards) was prepared from the 100 mg L^{-1} caffeine stock solution in water (100 µL in 10 mL). A 1 mg L^{-1} caffeine-$^{13}C_3$ working solution (for making calibration standards) was prepared from the 1 g L^{-1} caffeine-$^{13}C_3$ internal standard in methanol (25 µL in 25 mL). A 55 ug L^{-1} working solution of caffeine-$^{13}C_3$ internal standard (for adding to samples) was prepared from the 1 mg L^{-1} caffeine-$^{13}C_3$ working solution in methanol (550 µL in 10 mL).

E1 and EE2

1 g L^{-1} stocks of E1 and EE2 (dissolved in methanol) were obtained from Cerilliant Co. (Texas, USA). Estrogen isotope dilution standard (estradiol-$^{13}C_6$) solution was purchased from Cambridge Isotope Laboratories at a concentration of 100 µg mL^{-1} (100 mg L^{-1}). E1 and EE2 working solutions were prepared at 100 mg L^{-1} concentrations (for adding to samples) by spiking directly from the neat 1 g L^{-1} stocks in methanol. A 0.2 mg L^{-1} mixed working solution of E1 and EE2 (for making calibration standards) was prepared from the 100 mg L^{-1} working solutions of E1 and EE2 (50 µL of each in 25 mL). 1 mg L^{-1} estradiol-$^{13}C_6$ working solution (for making calibrations standards and adding to samples) was prepared from the 100 mg L^{-1} estradiol-$^{13}C_6$ stock solution in methanol (250 µL in 25 mL).

Reagents

Liquid chromatography-mass spectrometry (LC-MS) grade methanol, acetonitrile, and formic acid used for sample preparation and liquid chromatography-tandem mass spectrometry (LC-MS/MS) analyses were purchased from Fisher Scientific. Laboratory-grade water with a resistivity of 18.2 mΩ cm^{-1} and a total organic carbon (TOC) of < 5 µg L^{-1} was sourced from a Milli-Q purification system (Reference A+, Millipore) and used for the preparation of all chemical solutions and reagents.

2.5.2 Equipment Specifications

The bench-scale UV LED experiments were carried out using the 235 nm UV LED beam with narrow-band polychromatic emission wavelength ranging from 220 nm to 250 nm (peak wavelength of 235.3 nm), FWHM of 8.7 nm, radiant flux of 2.3 mW, and average E_0 of 65.5 µW cm^{-2} at 29.75 mm displacement from beam. The emittance spectrum of the beam is provided in Fig. 4. Irradiance measurements were performed using an Ocean Optics SR4 series miniature spectrometer (SR-4UVV240-50) equipped with a CC-3-DA cosine corrector. Absorbance and transmittance measurements were obtained using the Shimadzu LabSolutions UV-Vis spectrophotometer (model UV-2600i), and the molar absorbance spectrum of E1, E2, and caffeine are shown in Fig. 4.

2.5.3 Experimental Procedures

All experiments were conducted at room temperature (20–21°C). Experiment samples were prepared by spiking the required volume of the 100 mg L^{-1} E1, EE2, or caffeine stock solution into a 2 mM, pH 7 potassium phosphate buffer to achieve a target concentration of 10 ug L^{-1}. The buffer was adjusted to pH 7 using a combination of potassium phosphate monobasic (KH_2PO_4) and potassium phosphate dibasic (K_2HPO_4) at 2 mM concentrations. The bench-scale experimental set-up outlined in section 2.1 was implemented for all experiments. Experimental conditions, correction factors, and irradiance measurements at experiments start (t = 0) are provided in Table SI-8 in SI Text 12.

Samples were stirred constantly during treatment and equilibrated for a period of 5 minutes before starting experiments. For each experiment, a control sample was run under the same experimental conditions as the irradiated sample, but without any UV exposure. At each timepoint corresponding to target UV fluences (0–366 mJ cm^{-2} for E1, 0–732 mJ cm^{-2} for EE2, and 0–3305 mJ cm^{-2} for caffeine), including after sample equilibration period before any UV exposure (i.e., t = 0), aliquots were removed from the sample and associated control throughout the experiment and transferred to 2 mL amber autosampler vials. 100 µL volumes were aliquoted during the E1 and EE2 experiments, and 240 µL volumes were aliquot during the caffeine experiments, at each sampling timepoint. Directly after each aliquot was removed, the mass of the experimental sample was recorded to enable fluence determination using the trapezoid integration approach and evaporation correction of experimentally measured concentrations. Immediately after sampling and prior to LC/MS-MS analysis, samples were fortified with the 55 ug L^{-1} caffeine-$^{13}C_3$ internal standard solution to achieve a final concentration of 5 ug L^{-1} internal standard in sample. Similarly, all 100 µL aliquot samples in the 2 mL amber autosampler vials from the E1 and EE2 experiments were fortified with the 1 mg L^{-1} estradiol-$^{13}C_6$ internal standard solution to achieve a final concentration of 40 ug L^{-1} internal standard in sample.

2.5.4 Analytical Methods

All samples isolated from the bench-scale E1, EE2, and caffeine 235 nm UV LED experiments were analyzed via LC-MS/MS using an Agilent 1260 liquid chromatography system and an Agilent 6460 triple quadrupole mass spectrometer. Mass spectrometry acquisition of all compounds was conducted using multiple reaction monitoring (MRM) in either electrospray ionization (ESI) positive (caffeine) or negative (E1 and EE2) mode. Data acquisition and analysis were carried out using Agilent MassHunter software (version rev B.10.00). LC-MS/MS analysis details are provided in SI Text 13.

2.6 Declaration of AI Use

ChatGPT (OpenAI) was used to assist with language refinement and writing R code for regression model and visualization coding assistance in Section 2.3.2. All analyses were conducted using experimental data obtained by the authors. Any plots which generated using AI-assisted code were independently verified against equivalent plots produced in Microsoft Excel. The authors reviewed all outputs and take full responsibility for the accuracy and integrity of the reported results.

3.0 Results and Discussion

3.1 Evaluation of Revised Methods for Calculating Correction Factors for Determination of Average Fluence Rate ($\varvec{E}_{\varvec{a},\varvec{v},\varvec{g}}^{\varvec{\prime}}$)

The following section evaluates the alternative procedures proposed in section 2.2 for WF and DF determination. The proposed procedures were evaluated by comparing to standard methods outlined by Bolton & Linden (2003)[8]. A caffeine UV LED photodegradation study was used as a reference to evaluate the updated methods for WF and DF determination, with experimental details outlined in section 2.5. The calculation of other correction factors (i.e., PF, RF) was not evaluated in this section as their calculation method was not updated from standard approaches.

3.1.1 Water Factor

The method presented for WF determination when the UV LED is treated as a polychromatic light source (Eq. 5) was validated by comparing it to the WF calculated when the UV LED is treated as a monochromatic light source (Equation SI-1). The caffeine sample being irradiated had a transmittance of 99.8% (decadic absorption coefficient of a = 0.001 cm^{-1}) at the maximum 235 nm UV LED wavelength, and the depth l of the sample in the Petri dish was 2.2 cm. A 1 nm wavelength step-size was used to calculate the polychromatic WF. Based on these experimental parameters, only a 0.005% change in the WF results were observed when calculated using the polychromatic WF formula (0.9978) compared to the monochromatic WF formula (0.9977). This indicates a negligible change in WF when the polychromatic formula (Eq. 5) is used in comparison to the monochromatic formula (Equation SI-1) at the noted experimental conditions.

The negligible change between both WF formulas is likely attributed to the very low absorbance of the caffeine sample being irradiated (a = 0.001 cm^{-1}). Kheyrandish et al. (2018) demonstrated that the error associated with the monochromatic assumption for UV LED systems varies depending on sample absorption and relative UV LED emission spectrum, with minimal error observed for low absorbance samples and larger error observed for higher absorbance samples[10]. Therefore, the impact of the monochromatic WF approximation was further assessed in this study by comparing caffeine with furosemide, which was selected as it had both higher absorbance and greater wavelength-dependent variability across the 235 nm UV LED emission spectra (220–250 nm) (Figure SI-9 in SI Text 14). For the comparison concentrations evaluated (i.e., 0.005 mg mL^{-1} for caffeine and 0.011 mg mL^{-1} for furosemide), the decadic absorption coefficient of caffeine ranged from 0.069 cm^{-1} to 0.241 cm^{-1} over 220–250 nm, while that of furosemide ranged from 0.148 cm^{-1} to 1.037 cm^{-1} over the same wavelength range (Figure SI-9 in SI Text 14). Under these conditions, the monochromatic WF approximation resulted in a relative error of 0.6% for caffeine and 13.9% for furosemide, calculated relative to the polychromatic WF. These results demonstrate that greater sample absorbance and spectral variation across the UV LED emission spectrum can increase the error introduced by the monochromatic assumption. Therefore, the spectral characteristics of the target compound should be considered accordingly when evaluating WF calculation methods. Alternatively, the polychromatic WF may automatically be used as a conservative approach for UV LED systems.

3.1.2 Divergence Factor

The revised formula for DF determination (Eq. 7) was evaluated by comparing it against the formula proposed by Bolton & Linden (2003)[8] (Equation SI-8). As previously noted, a 54 mm diameter Petri dish and 50 mL sample was used for the caffeine validation experiments, with a total initial displacement of 29.75 mm between the sample surface and LED beam and 2.2 cm sample depth. Under these experimental conditions, the DF calculated using Eq. 7 (0.667) showed a 15.9% change when compared to the DF calculated using Equation SI-8 (0.575), consequently resulting in the same corresponding change in calculated E'_{avg} delivered during the experiment. This indicates that, in this scenario, using the standard Bolton & Linden (2003)[8] DF calculation would underestimate the calculated fluence by 15.9%. Figure 5 shows how the variability in both DF formulas changes with distance from the UV LED source for the 54 mm Petri dish diameter and 2.2 cm sample depth system used for this study. As expected, the variability between the two DF formulas decreased as the distance between the sample surface and UV LED beam increased, indicating that the system approaches near-collimated behaviour at greater source-to-sample distances. The relative error between the two DF formulas can also vary significantly depending on Petri dish diameters and sample depths, as demonstrated in SI Text 15.

The DF values calculated using the conventional (Equation SI-8) and revised (Eq. 7) formulas were also compared against the experimentally measured DF (Eq. 6) under the same experimental conditions. As detailed in SI Text 15, the experimentally measured DF was 0.675, differing by only 1.2% from the revised formula (Eq. 7), compared to a substantially larger difference of 14.8% from the conventional formula (Equation SI-8) at the noted experimental conditions.

3.2 Impact of Sample Loss on Determination of Average Fluence Rate ($\varvec{E}_{\varvec{a},\varvec{v},\varvec{g}}^{\varvec{\prime}}$)

The impact of sample loss was assessed for the UV LED photodegradation studies on E1, EE2, and caffeine. The average results for sample depth l, displacement L, E_0, WF, DF, and E'_{avg} from the triplicate E1, EE2, and caffeine experiments at the exposure times associated with different target fluences are outlined in Table SI-14 in SI Text 16. Figure SI-11 in SI Text 16 depicts the change in E'_{avg} delivered to the samples over exposure time, accounting for sample loss during the experiment. Note that exposure times were shorter for both E1 and EE2 due to their relative photosensitivity as compared to caffeine, which is relatively stable. The standard formula for WF (i.e., monochromatic, Equation SI-1) was used here as differences were negligible between the polychromatic and monochromatic WF formula at high sample transmittance (99.8%). As demonstrated by Figure SI-11 and Table SI-14 in SI Text 16, as sample time increases, sample depth decreases from sample evaporation (and, in this case, intermittent sampling over time). This results

in an increase in displacement and DF and subsequent decrease in E_0. Negligible change was observed in the WF results as path length decreased over experiment time (0.0029% for E1, 0.0104% for EE2, and 0.0641% for caffeine).

For E1, after 3.2 h exposure time (366 mJ cm^{-2} target fluence), a total of 1.3 mL sample was lost (45.9% from aliquoting and 54.1% from evaporation), resulting in a 0.6 mm increase in L, 2.9% drop in E_0, 1.2% increase in DF, and subsequent 1.7% decrease in $\mathrm{E}_{\mathrm{avg}}^{,}$ delivered to sample during the experiment. For EE2, after 6.5 h exposure time (732 mJ cm^{-2} target fluence), a total of 2.4 mL sample was lost (33.5% from aliquoting and 66.5% from evaporation), resulting in a 1.0 mm increase in L, 5.2% drop in E_0, 2.2% increase in DF, and subsequent 3.1% decrease in $\mathrm{E}_{\mathrm{avg}}^{,}$ delivered to sample during the experiment. For caffeine, after 30.2 h exposure time (3305 mJ cm^{-2} target fluence), a total of 14.7 mL sample was lost (11.5% from aliquoting and 88.5% from evaporation), resulting in a 6.4 mm increase in L, 26.6% drop in E_0, 13.7% increase in DF, and subsequent 16.5% decrease in $\mathrm{E}_{\mathrm{avg}}^{,}$ delivered to sample during the experiment. Comparative degradation studies on E1, EE2, and caffeine were conducted (section 3.3) to evaluate the level of impact this decrease in $\mathrm{E}_{\mathrm{avg}}^{,}$ delivered to the samples has on compound degradation kinetics.

3.3 Impact of Sample Loss on Fluence Determination Method and Compound Degradation Kinetics

The following section evaluates the impact of sample loss on the degradation kinetics of E1, EE2, and caffeine. Specifically, degradation kinetics were assessed using the proposed fluence determination method, which applies trapezoidal integration to account for changes in $\mathrm{E}_{\mathrm{avg}}^{,}$ delivered to sample over time (section 2.3.3), and evaporation correction of experimentally measured concentrations (section 2.4). This analysis provides insight into the importance of sample loss correction during UV degradation experiments and identifies conditions where sample loss corrections are necessary compared with cases where standard methods that do not account for sample loss remain reliable.

The combined effect of trapezoidal integration and evaporation correction are presented in Table 1 and Fig. 6, while the individual effects of each correction method are provided in Tables SI-15, SI-16, and SI-17 in SI Text 16. Only the caffeine results are depicted in Fig. 6 as sample loss effects were more significant for that experiment. The plots for E1 and EE2 are provided in the SI Text 16, presented by Figures SI-12 and SI-13, respectively. Overall, the evaporation correction method had a more significant impact on fluence-based rate constant (k_{obs}) compared to the trapezoidal fluence determination method alone. When both corrections were applied, the impact on k_{obs} varied among the three compounds depending on sample loss and compound photostability. For E1 (3.2 h exposure), k_{obs} increased from 48.2×10^{-4} cm^2 mJ^{-1} to 49.3×10^{-4} cm^2 mJ^{-1}, corresponding to a 2.1% difference relative to the uncorrected value. For EE2 (6.5 h exposure), k_{obs} increased from 18.3×10^{-4} cm^2 mJ^{-1} to 19.1×10^{-4} cm^2 mJ^{-1}, corresponding to a 4.6% difference relative to the uncorrected value. For caffeine (30.2 h exposure), k_{obs} increased from 0.615×10^{-4} cm^2 mJ^{-1} to 1.71×10^{-4} cm^2 mJ^{-1}, corresponding to a 93.9% difference relative to the uncorrected value. These results indicate that corrections for sample loss can substantially affect degradation kinetics and may be more pronounced for photostable compounds that require longer exposure times and therefore experience greater sample loss, like caffeine in this study.

Table 1

Percentage difference observed in fluence-based rate constants (k_{obs}) during the bench-scale UV LED studies on E1, EE2, and caffeine, before and after sample loss corrections were applied.

Compound	Target fluence (mJ cm^{-2})	Exposure time (h)	Drop in sample volume (%)	Drop in $\varrvec{E}_{\varrvec{avg}}^{,}$ (%)	Average $\varrvec{k}_{obs}$ (×10^{-4} cm^2 mJ^{-1})[a]		Difference in $\varrvec{k}_{obs}$ (%)[b]
					Uncorrected	Corrected	
E1	366	3.2	2.6	1.7	48.2 [28.8, 67.6]	49.3 [29.6, 68.9]	2.1
EE2	732	6.5	4.8	3.1	18.3 [13.0, 23.6]	19.1 [13.7, 24.5]	4.6
Caffeine	3305	30.2	29.1	16.5	0.615 [0.0907, 1.14]	1.71 [1.00, 2.41]	93.9

[a]Reported k_{obs} values are the mean from the triplicate experiments. Square brackets indicate 95% confidence intervals from the mean value, calculated on a normal distribution basis.

[b]Percentage difference were calcualted using unrounded average k_{obs} values.

Reported k_{obs} values in Figure B are the mean from the triplicate experiments.

3.4 Proposed Decision Framework for Fluence Determination and Sample Loss Correction in Near-Field Bench-Scale UV LED Experiments

Based on the results obtained in this work, a decision-based protocol was developed to guide fluence determination in bench-scale UV LED experiments, particularly for near-field systems where standard collimated-beam assumptions may not be valid. The protocol is intended to help determine whether standard fluence determination methods remain applicable or whether corrections to standard methods are required. The procedure first evaluates the

source-to-sample geometry, irradiance distribution across sample plane, and impact of polychromatic emission and sample loss to determine whether the set-up can be treated as quasi-collimated and standard fluence determination protocols apply. If near-field conditions are identified, and sample loss and incident angle effects are not negligible, the protocol guides the user through corrections necessary to account for these factors, as outlined in this work.

As shown in Fig. 7, the proposed procedure separates fluence determination into two main decision pathways. If the system satisfies assumptions of a quasi-collimated beam apparatus, standard fluence determination methods may be applied so long as irradiance distribution, polychromatic emission, and sample loss effects are negligible. However, if the system operates under near-field conditions, or if irradiance distribution does not satisfy standard protocol assumptions and sample loss is not negligible, the revised protocol should be used.

In this protocol, a ≤ 5% error in WF (resulting from monochromatic assumption and incident angle effects) and ≤ 1% error in RF (resulting from incident angle effects) were considered negligible. The ≤ 5% WF condition was taken from the US EPA guidance, which states that uncertainties in WF should not exceed 5% to maintain acceptable error in fluence measurements[31]. No specific acceptable-error threshold for RF was identified in bench-scale UV fluence determination literature. Therefore, a ≤ 1% relative error in RF was treated as negligible in this study. This is consistent with Kheyrandish et al. (2018) and Watanabe & Oguma (2023), who described RF differences within 1% as negligible[10,15]. Further, as outlined in Fig. 7, sample loss corrections are necessary when changes ≥ 5% in sample volume or $\mathrm{E}_{\mathrm{avg}}$ are observed during an experiment. This criterion was determined based on previous studies by Payne et al. (2025) and Bennett et al. (2025) where changes within 5% in $\mathrm{E}_{\mathrm{avg}}$ and sample volume were considered negligible during bench-scale UV studies, respectively.

In the context of this study, this would mean that sample-loss corrections are negligible for E1 (3% drop in sample volume and 2% drop in E'_{avg}; 2.1% difference in k_{obs} after correction), but necessary for EE2 (5% drop in sample volume and 3% drop in E'_{avg}; 4.6% difference in k_{obs} after correction) and caffeine (29% drop in sample volume and 17% drop in E'_{avg}; 93.9% difference in k_{obs} after correction). However, because the impact of sample loss on fluence and compound degradation kinetics can vary significantly depending on compound photostability, additional studies across a broader range of compounds are required to further define acceptable uncertainty in fluence-based chemical degradation rate constants, which may require revision of the sample loss correction criterion proposed in this study.

4.0 Conclusions

This study evaluated the limitations of conventional fluence determination methods when applied to near-field and long-exposure bench-scale UV LED systems and developed a revised framework for fluence determination and sample loss correction. The framework was evaluated using UV LED photodegradation studies on E1, EE2, and caffeine. Under the experimental conditions investigated, accounting for non-collimated irradiation resulted in a 15.9% change in E'_{avg} compared to when quasi-collimated conditions are assumed. The error from applying monochromatic approximation to calculate the WF was negligible under the low absorbance sample conditions investigated for this study, but effects were significantly more pronounced for samples demonstrating higher absorbance and absorbance variability across the LED emission spectrum. Sample loss emerged as an equally important consideration, particularly for long duration UV experiments. Results from this study showed that sample loss altered both the delivered fluence and measured contaminant concentrations, producing differences in k_{obs} ranging from only 2.1% for E1 to 93.9% for caffeine. The magnitude of this effect depended strongly on exposure duration, compound photostability, and the resulting volume loss. These findings suggest that previously published UV photolysis studies that did not account for sample loss may have more variability in reported fluence than initially thought. These considerations are especially impactful for degradation kinetics, particularly for experiments involving long exposure times and photostable contaminants.

Overall, the proposed framework provides a practical approach for evaluating fluence calculation assumptions and sample loss effects in bench-scale UV LED studies, rather than a complete optical model applicable to all reactor configurations. Further work should validate the approach using independent fluence measurements or chemical actinometry and evaluate its applicability across additional wavelengths, reactor configurations, sample depths, and water matrices. Future studies should also consider alternative reactor designs, such as closed or high-density array UV LED reactors, that would negate the need for these corrections in the first place. The framework developed here provides a step forward toward that transition by challenging the assumption that conventional mercury-lamp methods can be transferred directly to all UV LED systems and by providing a practical basis for designing, interpreting, and ultimately scaling future high-fluence UV LED treatment studies.

Declarations

Competing Interests

In accordance with journal disclosure policies, we acknowledge that Rich Simons is employed by Aquisense Inc. which provided partial funding for this work. The remaining authors declare no competing interests.

Author Contribution

RE: conceptualization, methodology, validation, formal analysis, investigation, data curation, writing – original draft, writing – review and editing, visualization. JB: conceptualization, methodology, writing – original draft, writing – review and editing. SM: conceptualization, methodology, writing – original draft, writing – review and editing. RS: conceptualization, methodology, formal analysis, writing – review and editing. AS: resources, writing – review and editing, supervision, funding acquisition. GG: conceptualization, resources, writing – review and editing, supervision, funding acquisition.

Acknowledgement

The authors would like to acknowledge funding from the Natural Sciences and Engineering Research Council (NSERC) Alliance “Partnership for Innovation in Climate Change Adaptation in Water & Wastewater Treatment” (grant ALLRP 568507-21), with supporting industry organizations: Halifax Water, LuminUltra Technologies Ltd., Cape Breton Regional Municipality, Mantech, Inc., City of Moncton, AquiSense Technologies, AGAT Laboratories, and CBCL Ltd.

Data Availability

The datasets generated and analyzed during the current study are available from the corresponding author on reasonable request.

References

1. Rauch, K. D. et al. A critical review of ultra-violet light emitting diodes as a one water disinfection technology. *Water Res. X*. **25**, 100271 (2024).
2. MacIsaac, S. A. et al. Improved disinfection performance for 280 nm LEDs over 254 nm low-pressure UV lamps in community wastewater. *Sci. Rep.* **13**, 7576 (2023).
3. Bennett, J. L. et al. Photolysis at the speed of light: chemical-free degradation of trace organic contaminants by bespoke photolysis using high-intensity ultraviolet C light-emitting diodes. *ACS ES&T Water*. **5**, 6375–6387 (2025).
4. MacIsaac, S. A. et al. UV LED wastewater disinfection: The future is upon us. *Water Res. X*. **24**, 100236 (2024).
5. Beck, S. E. et al. Evaluating UV-C LED disinfection performance and investigating potential dual-wavelength synergy. *Water Res.* **109**, 207–216 (2017).
6. Bennett, J. L., MacIsaac, S. A., Tchonlla, M., Sweeney, C. L. & Gagnon, G. A. Nitrate-mediated photooxidation of steroid estrogens: efficacy and prospects for wastewater treatment. *ACS ES&T Water*. **5**, 7326–7339 (2025).
7. Ray, H., Atkinson, A. J. & Full-Scale, U. V. L. E. D. Validation with Organism-Specific Dose Determination. *Environ. Sci. Technol.* **60**, 6725–6735 (2026).
8. Bolton, J. R. & Linden, K. G. Standardization of methods for fluence (UV dose) determination in bench-scale UV experiments. *J. Environ. Eng.* **129**, 209–215 (2003).
9. Bolton, J. R., Beck, S. & Linden, K. G. *Protocol for the Determination of Fluence (UV Dose) Using a Low-Pressure or Low-Pressure High-Output UV Lamp in Bench-Scale Collimated Beam Ultraviolet Experiments*. (2015). https://iuva.org/Guidance-Documents
10. Kheyrandish, A., Mohseni, M. & Taghipour, F. Protocol for determining ultraviolet light emitting diode (UV-LED) fluence for microbial inactivation studies. *Environ. Sci. Technol.* **52**, 7390–7398 (2018).
11. Li, J. et al. Combined UV LED and Chlorine for Synergistic Drinking Water Disinfection and Assessment of Disinfection By-Product Formation. *AWWA Water Sci.* **7**, e70046 (2025).
12. Rauch, K. D., MacIsaac, S. A., Stoddart, A. K. & Gagnon, G. A. UV disinfection audit of water resource recovery facilities identifies system and matrix limitations. *J. Water Process. Eng.* **50**, 103167 (2022).
13. Li, G. Q., Wang, W. L., Huo, Z. Y., Lu, Y. & Hu, H. Y. Comparison of UV-LED and low pressure UV for water disinfection: Photoreactivation and dark repair of Escherichia coli. *Water Res.* **126**, 134–143 (2017).
14. Lu, Y., Yang, B., Zhang, H. & Lai, A. C. Inactivation of foodborne pathogenic and spoilage bacteria by single and dual wavelength UV-LEDs: Synergistic effect and pulsed operation. *Food Control*. **125**, 107999 (2021).
15. Watanabe, S. & Oguma, K. A simple and practical method for fluence determination in bench-scale UV-LED setups. *Photochem. Photobiol*. **99**, 19–28 (2023).
16. Dóka, T. & Horák, P. Fluence and dose distribution modeling of an ultraviolet light disinfection process for pathogen inactivation efficiency evaluation. *ACS Omega*. **10**, 4291–4302 (2025).
17. Keshavarzfathy, M., Malayeri, A. H., Mohseni, M. & Taghipour, F. UV-LED fluence determination by numerical method for microbial inactivation studies. *J. Photochem. Photobiol., A*. **392**, 112406 (2020).
18. Rauch, K. D. *Examination of Measurement Techniques Used for Current and Emerging UV Treatment Technologies* (Dalhousie University, Halifax, Nova Scotia, 2018).
19. Rauch, K. D., Bennett, J. L., Stoddart, A. K. & Gagnon, G. A. UV LED disinfection as a novel treatment for common salmonid pathogens. *Sci. Rep.* **14**, 28392 (2024).
20. Woo, H. et al. Efficacy of inactivation of human enteroviruses by dual-wavelength germicidal ultraviolet (UV-C) light emitting diodes (LEDs). *Water* **11**, 1131 (2019).
21. Heyniger, N. et al. Mitigation of antibiotic resistance using ultraviolet light-emitting diodes for water treatment. *Environ. Eng. Sci.* **42**, 3–14 (2025).
22. Gilboa, Y., White, B., Shlomo, I., Linden, K. G. & Friedler, E. UV-LED irradiation for biofouling reduction in drip irrigation emitters fed with wastewater effluent. *Environ. Sci. : Water Res. Technol.* **10**, 2723–2735 (2024).
23. Yin, R. & Shang, C. Removal of micropollutants in drinking water using UV-LED/chlorine advanced oxidation process followed by activated carbon adsorption. *Water Res.* **185**, 116297 (2020).
24. Kwon, M. et al. Removal of sulfamethoxazole, ibuprofen and nitrobenzene by UV and UV/chlorine processes: A comparative evaluation of 275 nm LED-UV and 254 nm LP-UV. *Sci. Total Environ.* **637–638**, 1351–1357 (2018).

25. Li, G. Q., Huo, Z. Y., Wu, Q. Y., Lu, Y. & Hu, H. Y. Synergistic effect of combined UV-LED and chlorine treatment on Bacillus subtilis spore inactivation. *Sci. Total Environ.* **639**, 1233–1240 (2018).
26. Zou, X. Y. et al. Enhanced ronidazole degradation by UV-LED/chlorine compared with conventional low-pressure UV/chlorine at neutral and alkaline pH values. *Water Res.* **160**, 296–303 (2019).
27. Moreno, I. & Sun, C. C. LED array: Where does far-field begin? in *Eighth International Conference on Solid State Lighting* (eds Ferguson, I. T., Taguchi, T., Ashdown, I. E. & Park, S.-J.) 70580RSPIE, San Diego, California, USA, (2008). 10.1117/12.795944
28. Sholtes, K., Keliher, R. & Linden, K. G. Standardization of a UV LED peak wavelength, emission spectrum, and irradiance measurement and comparison protocol. *Environ. Sci. Technol.* **53**, 9755–9763 (2019).
29. Payne, E. M., Langelan, E. G. & Linden, K. G. High absorbance of nitrate leads to surprising effects on hydroxyl radical formation during 222 nm UV treatment. *Water Res.* **283**, 123754 (2025).
30. Elsebai, R. R code for UV LED beam irradiance decay modelling. (2026). https://doi.org/10.5281/zenodo.20635026
31. U.S. Environmental Protection Agency. *Ultraviolet Disinfection Guidance Manual for the Final Long Term 2 Enhanced Surface Water Treatment Rule*. (2006). https://www.epa.gov/system/files/documents/2022-10/ultraviolet-disinfection-guidance-manual-2006.pdf

Figures

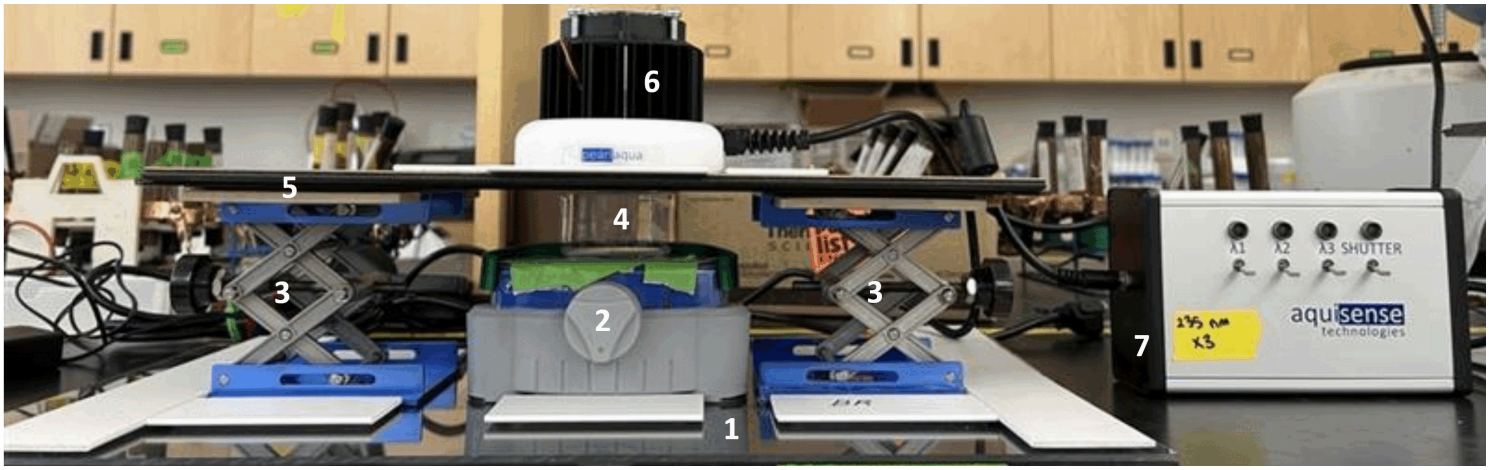


Figure 1

Photo of the bench-scale UV LED beam experimental set-up used for this study: (1) Apparatus base, (2) Stir plate, (3) Lab jacks for moving platform up/down, (4) Petri dish with sample, (5) Levelled plate to position beam above sample, (6) UV LED beam, (7) UV LED beam control panel.

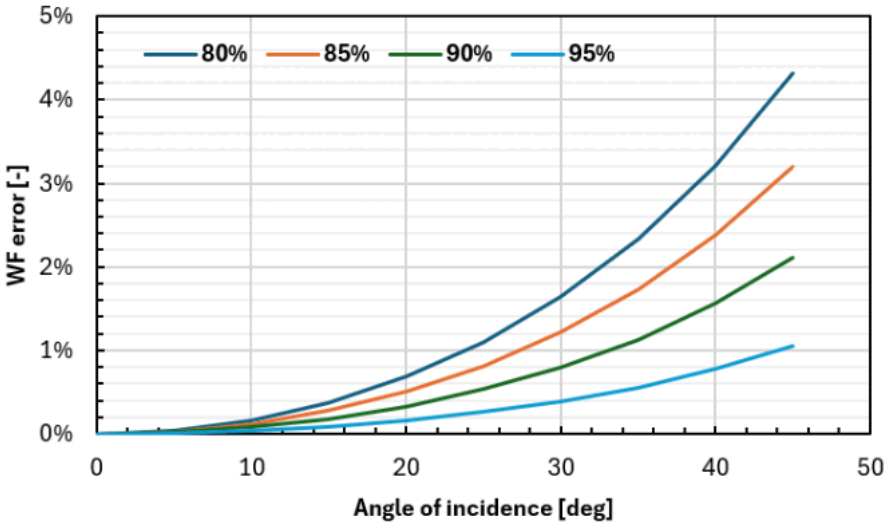


Figure 2

Plot showing effect of incident angle (0 - 45°) on the WF for a sample depth of 1 cm, expressed as the relative difference from normal incidence (0°). Legend values represent sample UV transmittance (UVT, %).

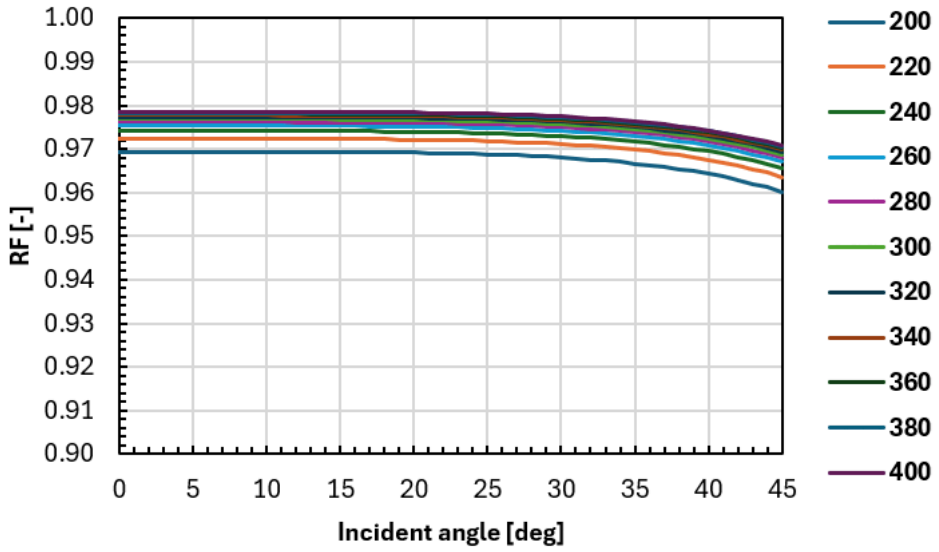


Figure 3

Plot of reflection factor (RF) against the angle of incidence of UV light on sample surface (0 – 45°) over wavelength range of 200 – 400 nm.

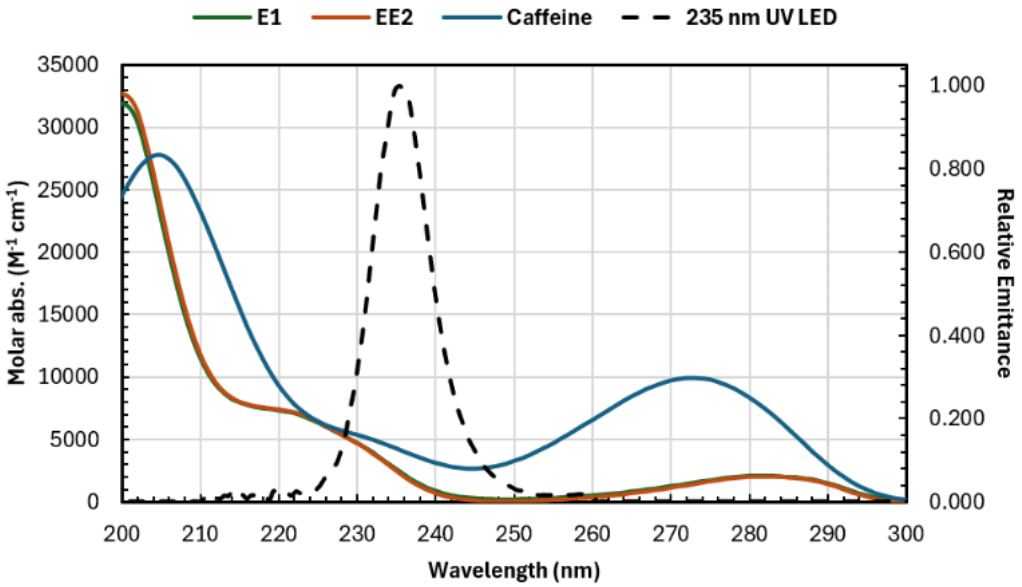


Figure 4

Relative emission spectrum of the 235 nm UV LED overlapped with the molar absorbance spectrums of E1, EE2, and caffeine.

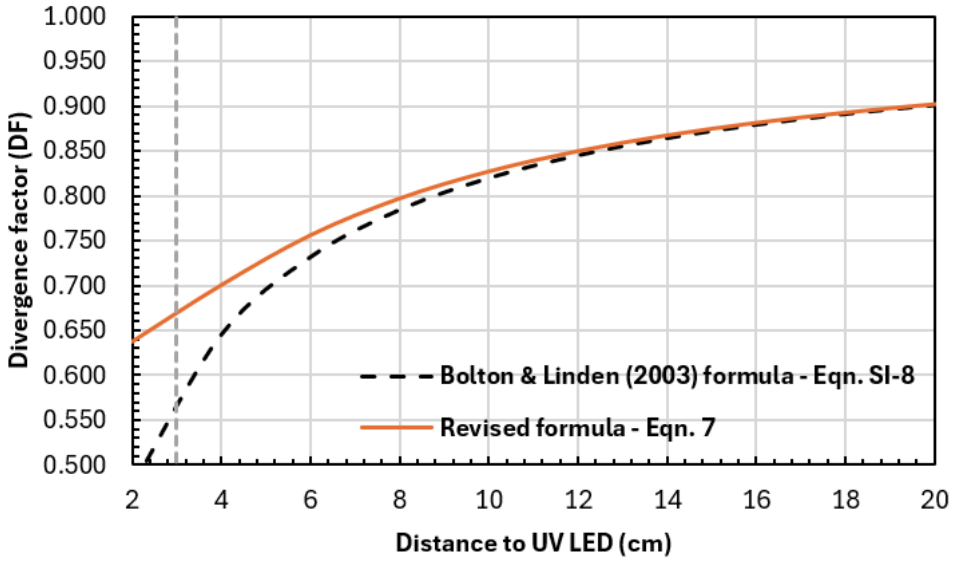


Figure 5

Plot showing variability between the standard DF formula for quasi-collimated systems (Equation SI-8) compared to the revised DF formula (Equation 7) accounting for non-collimated beam behaviour at different source-to-sample distances. Sample depth in 54 mm Petri dish was 2.2 cm. Vertical dashed grey line indicates source-to-sample distance at study condition (2.975 cm).

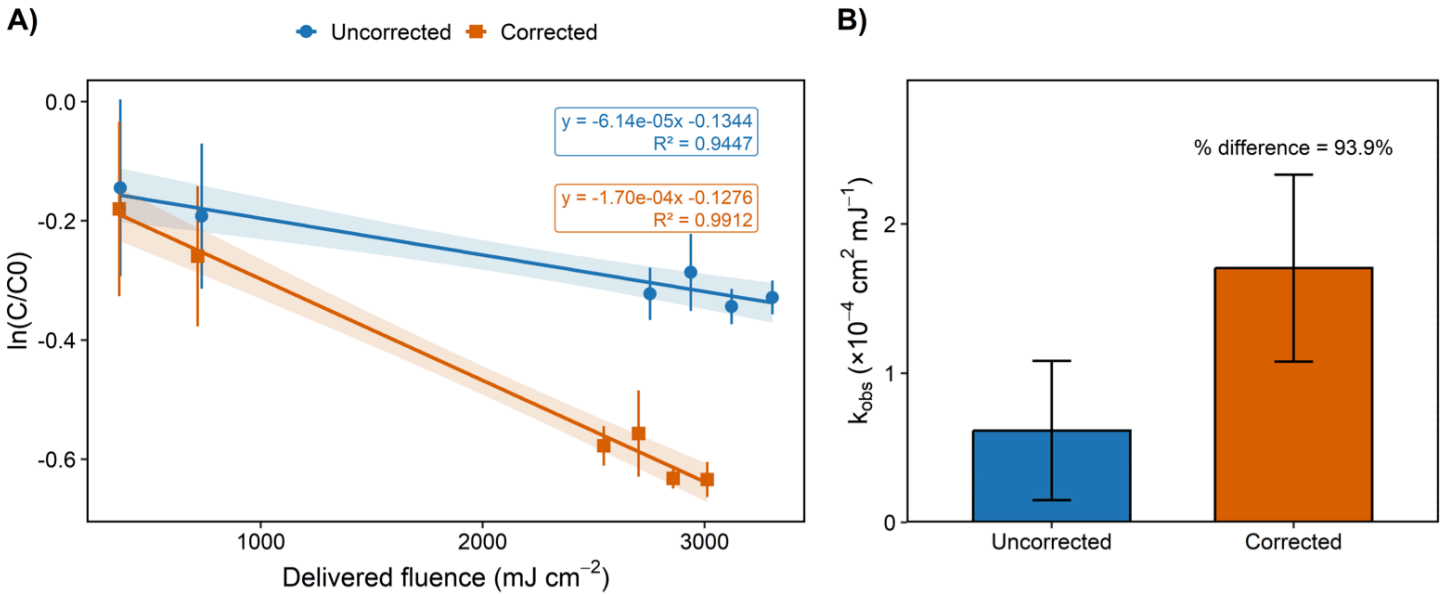


Figure 6

Caffeine first-order degradation kinetics plots (A) and bar plots showing difference in k_obs values (B) from accounting for sample loss in delivered fluence and sample concentration calculations (orange) compared to not accounting for sample loss (blue). Shaded regions represent the 95% confidence intervals of the fitted linear regression lines. Error bars represent one standard deviation from the mean value. Reported k_obs values in Figure B are the mean from the triplicate experiments.

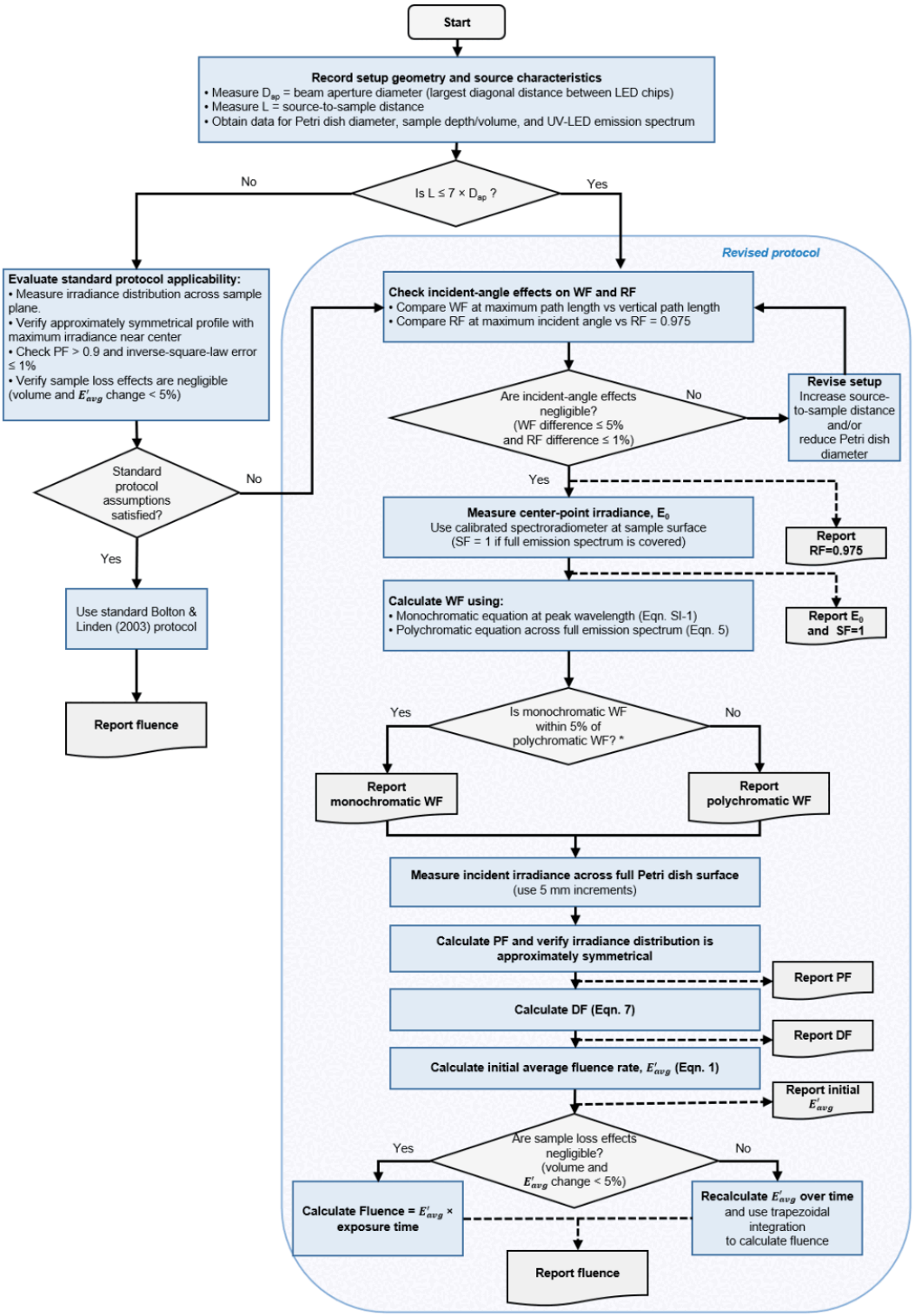


Figure 7

Proposed decision framework for fluence determination and sample loss correction in bench-scale UV LED studies.

Supplementary Files

This is a list of supplementary files associated with this preprint. Click to download.

- Elsebaietal.2026UVLEDMethodsManuscriptSupplementaryInformation.docx
- SupplementarySpreadsheetDetermiantionofCorrectionFactors.xlsx
- SupplementarySpreadsheetDeliveredUVFluenceTrapezoidIntegrationCalculator.xlsx